

Article

Temperature Dependence of the Elastic Modulus of $(\text{Ni}_{0.6}\text{Nb}_{0.4})_{1-x}\text{Zr}_x$ Membranes: Effects of Thermal Treatments and Hydrogenation

Oriole Palumbo ¹, Sergio Brutti ^{1,2}, Francesco Trequattrini ³, Suchismita Sarker ⁴, Michael Dolan ⁵, Dhanesh Chandra ⁴ and Annalisa Paolone ^{1,*}

¹ CNR-ISC, U.O.S. La Sapienza, Piazzale A. Moro 5, 00185 Roma, Italy;

E-Mails: oriole.palumbo@roma1.infn.it (O.P.); sergio.brutti@unibas.it (S.B.)

² Department of Science, University of Basilicata, Viale dell'Ateneo Lucano 10, 85100 Potenza, Italy

³ Department of Physics, Sapienza University of Rome, Piazzale A. Moro 5, 00185 Roma, Italy;

E-Mail: francesco.trequattrini@roma1.infn.it

⁴ Department of Chemical and Materials Engineering, University of Nevada, Reno, NV 89557, USA;

E-Mails: suchismita13994@gmail.com (S.S.); dchandra@unr.edu (D.C.)

⁵ CSIRO Energy Technology, Pullenvale, Queensland 4069, Australia;

E-Mail: Michael.Dolan@csiro.au

* Author to whom correspondence should be addressed; E-Mail: annalisa.paolone@roma1.infn.it; Tel.: +39-06-4991-4400; Fax: +39-06-4957-697.

Academic Editor: Craig M. Jensen

Received: 27 February 2015 / Accepted: 20 April 2015 / Published: 6 May 2015

Abstract: Amorphous $(\text{Ni}_{0.6}\text{Nb}_{0.4})_{1-x}\text{Zr}_x$ membranes were investigated by means of X-ray diffraction, thermogravimetry, differential thermal analysis and tensile modulus measurements. Crystallization occurs only above 673 K, and even after hydrogenation the membranes retain their mainly amorphous nature. However, after exposure to gaseous hydrogen, the temperature dependence of the tensile modulus, M , displays large variations. The modulus of the hydrogen reacted membrane is higher with respect to the pristine samples in the temperature range between 298 K and 423 K. Moreover, a sharp drop in M is observed upon heating to approximately 473 K, well below the glass transition temperature of these glasses. We propose that the changes in the moduli as a function of temperature on the hydrogenated samples are due to the formation of nanocrystalline phases of Zr hydrides in $(\text{Ni}_{0.6}\text{Nb}_{0.4})_{1-x}\text{Zr}_x\text{-H}$ membranes.

Keywords: amorphous membranes; hydrogenation; elastic modulus; X-ray diffraction (XRD); differential thermal analysis (DTA); thermogravimetric analysis (TGA)

1. Introduction

Alloy membranes with hydrogen selective properties have broad technological applications in the field of hydrogen production and purification [1–3]. Usually, thin, crystalline, Pd-based membranes are used for the purification of hydrogen due to their high permeability to hydrogen ($\sim 2.0 \times 10^{-8} \text{ mol m}^{-1} \text{ s}^{-1} \text{ Pa}^{-0.5}$ for Pd₇₅Ag₂₅) and selectivity [4]. The operating temperatures of these membranes are higher than 573 K. Palladium, however, is an expensive and scarce element, therefore inexpensive and abundantly available alloys are being investigated as a replacement. Amorphous alloy membranes show promising properties [5], such as excellent mechanical strength, high thermal stability and soft magnetic properties [6–8].

A promising class of amorphous alloy membranes are the Ni-Zr or Ni-Nb-Zr ones. Hara *et al.* reported that Ni-Zr based alloys are stable, and do not become brittle in the temperature range between 473 K to 623 K while the hydrogen permeability of the Ni₆₄Zr₃₆ sample is of the order of $10^{-9} \text{ mol m}^{-1} \text{ s}^{-1} \text{ Pa}^{-0.5}$ [9–11]. Later studies showed that the hydrogen permeability of Ni-Nb-Zr amorphous samples is significantly enhanced by the addition of Zr to the alloys, reaching a permeability comparable to that of the Pd-based alloys, on the order of 10^{-9} – $10^{-8} \text{ mol m}^{-1} \text{ s}^{-1} \text{ Pa}^{-0.5}$ [12–16].

The Ni-Nb-Zr membranes can be produced in the amorphous state by various techniques, such as planar flow cast or melt spinning. These amorphous alloys are stable at operating temperatures up to 623 K, but devitrify at temperatures higher than 780 K. In the Ni-Zr and Ni-Nb-Zr systems the crystallization temperature (T_x) decreases as the Zr content increases [15,17]; for example the $T_x \sim 843$ K for Ni_{63.7}Zr_{36.3}, that decreases to $T_x \sim 653$ K for Ni₃₀Zr₇₀. Another example is that of Ni₆₀Nb₄₀ with a $T_x \sim 943$ K which decreases to $T_x \sim 843$ K with the addition of 30 at.% Zr (*i.e.*, in the alloy (Ni_{0.6}Nb_{0.4})₇₀Zr₃₀). Permeation tests on Ni-Nb-Zr amorphous alloys are usually conducted in the temperature range of 673–723 K [12–16]; the permeability of Pd (1.8 – $2.0 \times 10^{-8} \text{ mol m}^{-1} \text{ s}^{-1} \text{ Pa}^{-0.5}$) [14] is slightly higher than that of our alloys (Ni_{0.6}Nb_{0.4})₇₀Zr₃₀ ($1.4 \times 10^{-8} \text{ mol m}^{-1} \text{ s}^{-1} \text{ Pa}^{-0.5}$) at 723 K and of (Ni_{0.6}Nb_{0.4})₈₀Zr₂₀ ($8 \times 10^{-9} \text{ mol m}^{-1} \text{ s}^{-1} \text{ Pa}^{-0.5}$) at 673 K [14]. Typically, in a laboratory these experiments take one to two weeks during which the membranes are at elevated temperatures and are exposed to hydrogen. To terminate the experiment, it is important that all the hydrogen be desorbed from the membrane before cooling down to room temperature. If all the hydrogen is not removed, these membranes have a propensity to embrittle. The embrittlement of the samples with or without hydrogen is heavily influenced by their elastic properties, therefore, in this paper we investigate the changes of the elastic modulus of (Ni_{0.6}Nb_{0.4})_{1-x}Zr_x membranes induced by thermal treatments and hydrogenation. One of the property we are interested is in the amorphous to amorphous phase transitions as a function of temperature.

2. Results

Two pristine membranes were investigated in the present study: (1) $(\text{Ni}_{0.6}\text{Nb}_{0.4})_{70}\text{Zr}_{30}$, thereafter referred to as Zr₃₀, and $(\text{Ni}_{0.6}\text{Nb}_{0.4})_{80}\text{Zr}_{20}$ as Zr₂₀. The effect of thermal treatments and/or hydrogenation on these two specimens will be determined. X-ray diffraction (XRD) data of the membranes are reported in Figure 1. The starting materials display a broad peak centered around 39.9° in Zr₂₀ and 39.3° in Zr₃₀, which confirms the mainly amorphous nature of the pristine membranes.

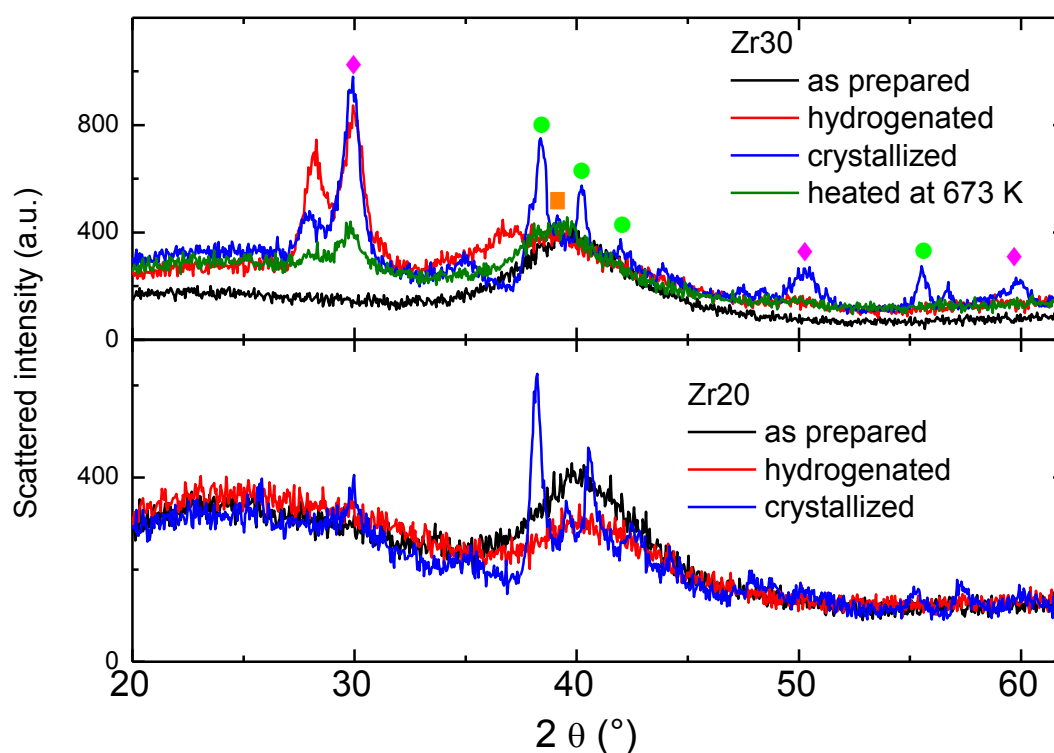


Figure 1. X-ray diffraction (XRD) spectra of all samples with attribution to crystalline phases (magenta diamonds: ZrO_2 ; green solid circles: $\text{Ni}_{10}\text{Zr}_7$; orange squares: $\text{Ni}_{48}\text{Zr}_{52}$) [18–22].

Differential thermal analysis (DTA) measurements (in Figure 2) show the crystallization temperature. Two sharp peaks at 816 and 836 K, were observed for the Zr₃₀ alloy, whereas Zr₂₀ sample displayed one peak at ~ 868 K. We attribute these peaks to the crystallization process of the amorphous alloys, in agreement with previous reports [14,15,17]. The crystallization of Zr₃₀ sample is a multistep process, as suggested by the weak structures (peaks) present in the DTA signal. A multistep crystallization is very common in amorphous alloys for hydrogen storage. It is worth noting that the temperatures at which our samples display the highest peaks of the DTA signals well agree with the known crystallization temperatures of the two alloys: $T_x \sim 876$ K for the Zr₂₀ and 808 K for the Zr₃₀ alloy [15].

The occurrence of the crystallization process at high temperatures is confirmed by XRD data collected on samples Zr₃₀ and Zr₂₀ heated to 973 K in an argon environment (Figure 1). In Zr₃₀ sample Bragg peaks are observed after such thermal treatments at ~ 38.4 , 40.2 , 42.1 and 55.5° 2θ that have been ascribed to $\text{Ni}_{48}\text{Zr}_{52}$ phase [21], and Bragg peak located at 39.2° 2θ , that may possibly be due to the presence of $\text{Ni}_{10}\text{Zr}_7$ phase [22]. Note that the Bragg peaks of ZrO_2 are due to the exposure of the

sample to air for XRD experiments [18–20]. The Zr20 sample displays similar characteristics when heated to 973 K. For the sake of completeness we also heated a Zr30 sample only up to 673 K for 8 h in an argon atmosphere. In the case of the Zr30 sample heated to 673 K, (much lower than the $T_x \sim 816$ K for Zr30), the XRD pattern shows the characteristic broad amorphous hump at $\sim 40^\circ 2\theta$, and a minor peak at 30.2° , ascribed to ZrO_2 .

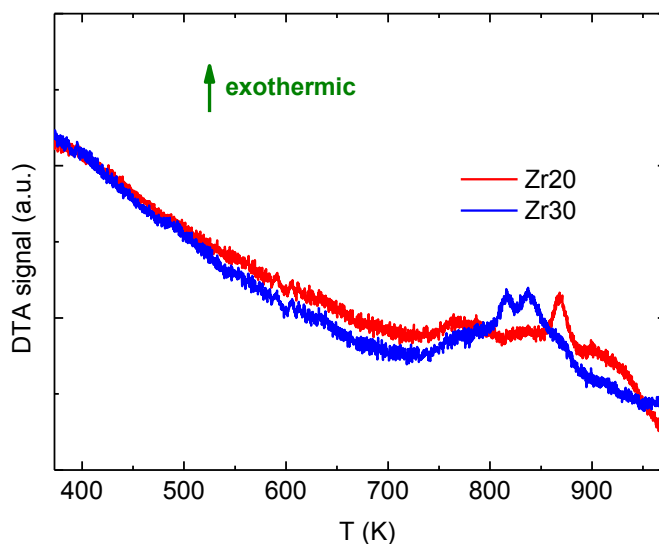


Figure 2. Differential thermal analysis (DTA) measurements on the two amorphous membranes conducted with a temperature rate of 4 K/min after subtraction of the background records with empty crucibles.

In order to check whether the hydrogenation process can induce crystallization, the membranes with the two different content of Zr were hydrogenated at 673 K by using a home-made Sieverts apparatus, starting with an initial hydrogen pressure of ~ 0.55 MPa. The hydrogenation process for Zr30 lasted 4 h, and 22 h for Zr20; with a final hydrogen content of ~ 0.4 wt%H for Zr20 and ~ 0.8 wt% H for Zr30, after which the experiments were terminated. In Figure 1 the high intensity Bragg peaks around $40^\circ 2\theta$ are retained in the hydrogenated samples, and therefore after hydrogenation the specimens remain mainly amorphous (see Figure 1). Only the hydrogenated Zr30 sample displays two Bragg peaks at 28.3 and $29.9^\circ 2\theta$ due to the formation of ZrO_2 [18–22].

Dynamical Mechanical analysis (DMA) results yielded interesting results; the tensile modulus values, M , measured from the room temperature to 673 K are shown in Figure 3. At room temperature the tensile modulus of Zr20 ($M = 1.0 \times 10^{10}$ Pa) is higher than that of Zr30 ($M = 6.5 \times 10^9$ Pa). The modulus decreases almost linearly up to 503 K for the Zr20 and up to 543 K for the Zr30 sample, showing a strong decrease of M by a factor of ~ 2 which is clearly visible. In another region of the spectrum above ~ 633 K one can observe, again, a much smoother linear decrease of the modulus. An almost linear decrease of the elastic modulus with increasing temperature is usually observed in many solids and can be explained by the Debye theory [23].

We could not measure the tensile modulus of samples in which a full crystallization was induced by a thermal treatment in argon at 923 K in the thermobalance, because the membranes become so fragile that they break as soon as they are mounted in the clamps of the Dynamic Mechanical Analyzer

(DMA) used for the elastic modulus measurements. Therefore a direct comparison of the elastic properties of the crystallized samples could not be performed.

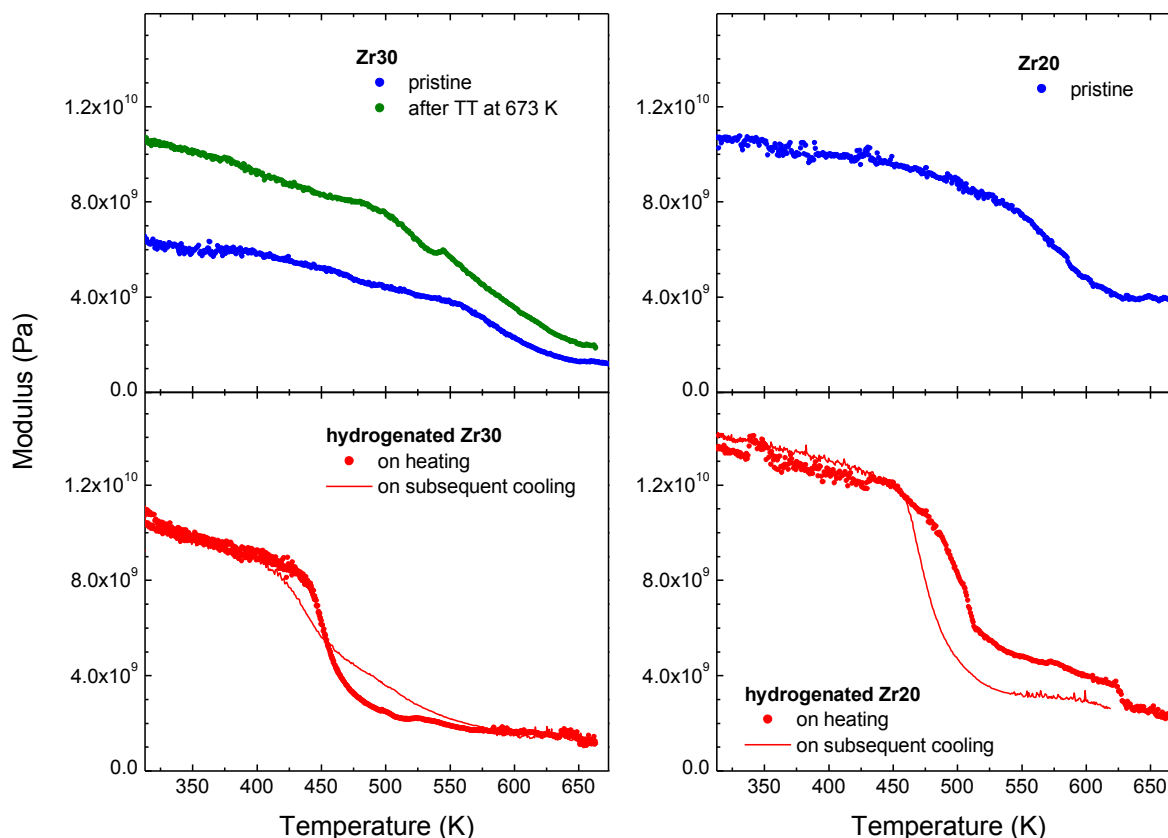


Figure 3. Dynamic Mechanical Analyzer (DMA) measurements of the membranes.

DMA measurements were repeated on the hydrogenated membranes. They were more fragile than the starting materials and in some cases small pieces of the hydrogenated samples broke up before measurements. In order to be sure that the hydrogenated membranes do not break during measurements we carefully measured the elastic moduli both on heating and cooling, comparing the values of M along the thermal cycle and checking that no sudden and irreversible change of the elastic modulus occurred. These DMA measurements of the hydrogenated membranes are reported in Figure 3. One can note that for both Zr concentrations the elastic modulus at room temperature and below 423 K is higher in hydrogenated samples than in the starting materials. Upon heating above the room temperature, M decreases almost linearly up to ~ 393 K for Zr30, and up to ~ 423 K for Zr20. Above such temperatures, M displays a strong and sharp decrease by a factor 3–4. For both samples such variation occurs in a very limited temperature range, 423 K to 673 K for the Zr30, and 443 K to 523 K for the Zr20 sample. For both specimens a smooth linear decrease of M is observed above 523 K.

The appearance of an abrupt decrease of M is strictly due to the presence of hydrogen in the hydrogenated samples and cannot be explained as an effect of the thermal cycle used during hydrogenation (in our case, heating at 673 K for at least 4 h). The proof of this comes from a measurement performed on a piece of the Zr30 membrane heated at 673 K for 8 h (sample Zr30_TT) in an argon atmosphere (a longer thermal treatment than that used for the hydrogenation process at the same temperature). Zr30_TT shows a smooth increase of the modulus, without the abrupt change

presented by the hydrogenated membrane (see Figure 3). Indeed, the temperature dependence of M for sample Zr30_TT strictly resembles that of the pristine membrane, except that the absolute value is slightly higher. This increase of the absolute value of M in the thermally treated specimen can be possibly due the formation of nanometric crystallites, not detected by X-ray diffraction because of their small dimensions, whose presence increases the elastic stiffness of the sample.

The tensile modulus of the hydrogenated samples measured on subsequent cooling, after heating to 673 K, (in the Figure 3) again shows strong variations between 423 K and 523 K for the Zr30, and between 443 K to 523 K for the Zr20 sample. In the case of the Zr20 sample this feature stretches to a broader temperature range than the Zr30 sample with the modulus jump clearly visible.

To confirm if the hydrogenated sample are not completely desorbed, thermogravimetric analyses (TGA) measurements were performed on the hydrogenated Zr30 samples. Results show that hydrogen was not completely released by heating at 673 K as shown in Figure 4. The hydrogen gas starts to release above 473 K but there is incomplete dehydrogenation below ~ 873 K. One can note that above 873 K (Figure 4) the sample starts to oxidize, and the mass increases. For both the Zr20 and the Zr30 samples half of the initial hydrogen content is retained after thermal treatments up to ~ 673 K.

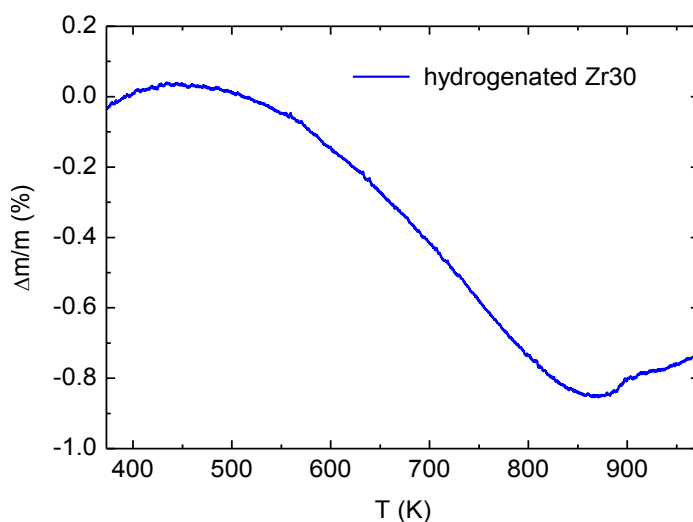


Figure 4. TGA scan of the hydrogenated Zr30 sample.

3. Discussion

A striking difference between the elastic moduli variation of the pristine (unhydrogenated) and the hydrogenated membranes is evident in Figure 3. In the hydrogenated Zr30 membrane we observe an abrupt decrease of the elastic modulus in an extremely limited range of 423 K to 473 K, and 443 K to 523 K for the Zr20 membrane sample. Such variations are completely absent in the pristine materials and they resemble the modulus changes occurring concomitantly with a phase transition. Indeed, no change in the shape and position of the modulus drop are visible when measurements are conducted with different frequencies (results not shown). Conversely, if the modulus drop was due to a thermally activated process, one would observe a shift of the modulus variations toward higher temperatures when M was measured at higher frequency [23,24].

Usually, these materials display a gradual decrease of the elastic modulus with increasing temperature [23]. However, materials undergoing phase transitions display strong deviations from such a trend and present sharp changes of M as a function of temperature around the phase transition temperature. Elastic moduli typically display remarkable variations in correspondence of phase transitions, independently of their order [24]. It should be noted that the DSC or DTA can easily detect first order phase transitions and measure latent heats of phase transitions, but are not well suited to detect phase transitions of the second or higher order; for these DMA measurements are critical.

The XRD measurements indicate that both the pristine and the hydrogenated $(\text{Ni}_{0.6}\text{Nb}_{0.4})_{1-x}\text{Zr}_x$ membranes investigated in the present study are mainly amorphous. However, some studies of similar samples indicate that at the microscopic level they are not completely amorphous: they actually possess some nano-crystalline inclusions [16,25,26]. Such nano-crystals are too small and diluted to cause a detectable diffraction signal in standard diffractometers [16,25,26]. Indeed, TEM analysis of $\text{Ni}_{64}\text{Zr}_{36}$ samples pointed out that after thermal treatments the surface shows the presence of fine precipitates, 500 nm in diameter, with a high concentration of Ni [16]. Moreover, some blistering possibly due to the precipitation of γ -ZrH was observed [16]. Also Jayala Kshmi *et al.* reported that nano-crystallization takes place in hydrogenated Zr- and Ni- based glasses, even though XRD is unable to detect crystalline precipitates [25,26]. Indeed, electron diffraction patterns show the formation of nanocrystals of γ -ZrH after hydrogenation the $\text{Zr}_{50}\text{Ni}_{27}\text{Nb}_{18}\text{Co}_5$ alloy, with dimensions of the order of ~ 2 nm and the formation of the Ni_2H phase in $\text{Ni}_{59}\text{Zr}_{16}\text{Ti}_{13}\text{Nb}_7\text{Sn}_3\text{Si}_2$ [26].

In view of this framework, we suggest that the modulus variation in the hydrogenated samples around 473 K is due to the formation on cooling of nanometric Zr hydride or its dissolution on heating. Indeed, Zr is an energy favorable site for the absorption of hydrogen, as pointed out for example by XAFS measurements and molecular dynamics simulations [27]. We suggest that in the Zr rich zones of the samples, hydrogen can form a solid solution with the Zr atoms. However, as temperature is decreases the solid solution undergoes a phase transition to a new stable hydride phase. On heating, the process is reversible. The Zr-H phase diagram [28,29] presents two regions with phase transitions in the temperature range around 473 K: the two lines defining the separation between the α and δ phases and the coexistence region between the δ hydride phase and α -Zr phase. We suggest that the modulus variations reported in Figure 3 correspond to the transition from the solid solution to the hydride on cooling and from the stable hydride to the solid solution on heating. Some modulus variations due to hydride formation and dissolution have also been previously observed in other Zr alloys, such as Zircaloy-4 or Zr-2.5Nb [30,31].

TGA measurements indicate that at least half of the hydrogen initially present in the samples is liberated after a thermal treatment at 673 K. On the other side DMA measurements find a reasonable recovery of the elastic modulus after the same thermal treatment. These results are not in contrast in view of the attribution of the modulus drop to the formation and dissolution of Zr hydride. Indeed Zr hydride is only a minority phase, whose presence is detected by DMA measurements. As Zr atoms are the energy preferred sites for absorption of hydrogen, Zr-H is the most stable of the hydride phases in the sample and therefore it will be the least affected by dehydrogenation. Therefore a partial release of hydrogen from the samples does not affect the presence of the Zr hydride.

In summary, we suggest that the present measurements of the elastic modulus of hydrogenated membranes strongly indicate that nanometer size Zr hydride can form or dissolve as a function of

temperature and therefore the elastic properties of the amorphous materials display a dramatic variation around 473 K. In this way the modulus measurements become an easily way to detect the presence of nanocrystalline Zr hydrides.

4. Experimental Section

Crystalline $(\text{Ni}_{0.6}\text{Nb}_{0.4})_{100-x}\text{Zr}_x$ ($x = 20$ and 30) alloy ingots were prepared by arc melting in a purified Ar atmosphere. Amorphous ribbons ~ 100 μm thick and 30 mm wide have been prepared using the melt-spinning method [15].

Simultaneous TGA-DTA measurements were conducted by means of a Setaram Setsys Evolution 1200 TGA system (Caluire, France) [32]. The furnace was continuously flooded with high purity argon (60 ml/min). For each experiment a sample mass of ~ 10 mg was used.

XRD have been recorded at room temperature by using an X-Pert PANalytical theta-theta diffractometer (Almelo, The Netherlands) in the range 10 – 70° with a step of 0.025° , time/step = 3 s. Millimetric pieces of the membranes have been spread on the planar glass holder and then measured in the XRD chamber.

Dynamic Mechanical Analysis (DMA) was carried out on small membrane pieces 4–6 mm wide and 10–12 mm long by using a DMA 8000 (Perkin Elmer, Waltham, MA, USA) in the so-called “tension configuration” [33–35]. The storage modulus, M , was measured at frequencies of 1 and 10 Hz between room temperature and 673 K, that is the maximum temperature allowed by the system. All measurements were carried out in a flux of pure argon to prevent oxidation of samples. In order to directly compare DTA and DMA measurements, we conducted the two experiments at the same temperature rate (4 K/min).

Hydrogenation of the samples was obtained by means of a home-made Sieverts apparatus working up to a 20 MPa pressure and a 773 K temperature [36]. The amount of hydrogen exchanged between the gas atmosphere and the solid samples is measured by the pressure variation in calibrated cylinders connected by Swagelok tubes to the reaction chamber where the sample is placed. A homemade computer program developed in the Labview language is used to acquire the time evolution of the pressure detected by two micro-Baratron transducers working between 0 and 0.7 MPa and between 0 and 20 MPa, respectively, and of the temperature of the five cylinders and of the tubes connecting the cylinders and the reaction chamber. The real gas state equation is used to calculate the exchanged hydrogen moles. For all samples we chose to conduct hydrogenation processes at $T = 673$ K and $p \approx 0.55$ MPa, because these are the temperature and pressure at which the membranes have practical application in gas reactors in order to separate H_2 from other gases. We extended the hydrogenation procedure until a steady state was obtained and no more hydrogen was absorbed by the membranes. The Zr30 sample, exposed to $p \approx 0.55$ MPa, absorbs more hydrogen and in a shorter time than the Zr20 specimen. After only 4 h, Zr30 reaches a hydrogen concentration value of 0.8 wt%. On the contrary, in the same conditions, Zr20 absorbs only 0.4 wt% even after 22 h.

5. Conclusions

XRD measurements indicate that $(\text{Ni}_{0.6}\text{Nb}_{0.4})_{100-x}\text{Zr}_x$ ($x = 20$ and 30) membranes are mainly in an amorphous state both when prepared by means of melt spinning, and after hydrogenation at 673 K.

However, the elastic modulus of the hydrogenated samples display a strong and sharp decrease that occurs in an extremely limited range between 423 K and 473 K for the Zr30 and 443 K to 523 K for the Zr20 sample. We suggest that these features are due to the dissolution on heating and to the formation on cooling of nanocrystalline Zr hydride. It is suggested that the DMA analysis is a method to detect the presence of nanocrystalline crystalline phases and possible local atomic order changes in the amorphous solids, such as the membranes.

Acknowledgments

This research has been partially supported by the Project FIRB 2010- Futuro in Ricerca “Hydrides as high capacity anodes for lithium ion batteries” funded by the Italian Ministry of Research. One of the authors (D.C.) would like to thank U.S. Department of Energy, Grant No. DE-NA-0002004 for the support of this project. Thanks are due to Prof. A. Colella and Prof. G. Mongelli for the diffraction experiments.

Author Contributions

Suchismita Saker, Michael Dolan and Dhanesh Chandra synthesized the samples. Sergio Brutti performed the XRD measurements. Oriele Palumbo, Francesco Trequattrini and Annalisa Paolone performed the DMA, TGA and DTA measurements. Annalisa Paolone and Dhanesh Chandra wrote and later edited, the manuscript.

Conflicts of Interest

The authors declare no conflict of interest.

References

1. Dolan, M.D. Non-Pd BCC alloy membranes for industrial hydrogen separation. *J. Membr. Sci.* **2010**, *362*, 12–28.
2. Hwang, K.; Lee, C.; Ryi, S.; Lee, S.; Park, J. A multi-membrane reformer for the direct production of hydrogen via a steam-reforming reaction of methane. *Int. J. Hydrog. Energy* **2011**, *37*, 6601–6607.
3. Paglieri, S.N.; Way, J.D. Innovations in palladium membrane research. *Sep. Purif. Rev.* **2002**, *31*, 1–169.
4. Serra, E.; Kemali, M.; Perujo, A.; Ross, D.K. Hydrogen and deuterium in Pd-25pct Ag alloy: Permeation, diffusion, solubilization, and surface reaction. *Metall. Mater. Trans. A* **1998**, *29A*, 1023–1028.
5. Dolan, D.M.; Dave, N.C.; Ilyushech Kin, A.Y.; Morpeth, L.D.; McLennan, K.G. Composition and operation of hydrogen-selective amorphous alloy membranes. *J. Membr. Sci.* **2006**, *285*, 30–55.
6. Zhang, T.; Inoue, A. Thermal and mechanical properties of Ti-Ni-Cu-Sn amorphous alloys with a wide supercooled liquid region before crystallization. *Mater. Trans. JIM* **1998**, *39*, 1001–1006.

7. Kimura, H.; Inoue, A.; Yamaura, S.I.; Sasamori, K.; Nishida, M.; Shinpo, Y.; Okouchi, H. Thermal stability and mechanical properties of glassy and amorphous Ni-Nb-Zr alloys produced by rapid solidification. *Mater. Trans. JIM* **2003**, *44*, 1167–1171.
8. Inoue, A.; Koshiba, H.; Zhang, T.; Makino, A. Wide supercooled liquid region and soft magnetic properties of Fe₅₆Co₇Ni₇Zr_{0–10}Nb (or Ta)_{0–10}B₂₀ amorphous alloys. *J. Appl. Phys.* **1998**, *83*, 1957–1974.
9. Hara, S.; Hatakeyma, N.; Itoh, N.; Kimura, H.M.; Inoue, A. Hydrogen permeation through amorphous Zr_{36–x}Hf_xNi₆₄ alloy membranes. *J. Membr. Sci.* **2003**, *211*, 149–156.
10. Hara, S.; Sakaki, K.; Itoh, N.; Kimura, H.M.; Asami, K.; Inoue, A. An amorphous alloy membrane without noble metals for gaseous hydrogen separation. *J. Membr. Sci.* **2000**, *164*, 289–294.
11. Hara, S.; Hatakeyma, N.; Itoh, N.; Kimura, H.M.; Inoue, A. Hydrogen permeation through palladium-coated amorphous Zr-M-Ni (M = Ti, Hf) alloy membranes. *Desalination* **2002**, *144*, 115–120.
12. Yamaura, S.I.; Shimpo, Y.; Okouchi, H.; Nishida, M.; Kajita, O.; Kimura, H.; Inoue, A. Hydrogen permeation characteristics of melt-spun Ni-Nb-Zr amorphous alloy membranes. *Mater. Trans. JIM* **2003**, *44*, 1885–1890.
13. Yamaura, S.I.; Sakurai, M.; Hasegawa, M.; Wakoh, K.; Shimpo, Y.; Nishida, M.; Kimura, H.; Matsubara, E.; Inoue, A. Hydrogen permeation and structural features of melt-spun Ni-Nb-Zr amorphous alloys. *Acta Mater.* **2005**, *53*, 3703–3711.
14. Paglieri, S.N.; Pal, N.K.; Dolan, M.D.; Kim, S.M.; Chien, W.M.; Lamb, J.; Chandra, D.; Hubbard, K.M.; Moore, D.P. Hydrogen permeability, thermal stability and hydrogen embrittlement of Ni-Nb-Zr and Ni-Nb-Ta-Zr amorphous alloy membranes. *J. Membr. Sci.* **2011**, *378*, 42–50.
15. Kim, S.M.; Chandra, D.; Pal, N.K.; Dolan, M.D.; Chien, W.M.; Talekar, A.; Lamb, J.; Paglieri, S.N.; Flanagan, T.B. Hydrogen permeability and crystallization Kinetics in amorphous Ni-Nb-Zr alloys. *Int. J. Hydrog. Energy* **2012**, *37*, 3904–3913.
16. Adibhatla, A.; Dolan, M.D.; Chien, W.; Chandra, D. Enhancing the catalytic activity of Ni-based amorphous alloy membrane surfaces. *J. Membr. Sci.* **2014**, *463*, 190–195.
17. Kim, S.M.; Chien, W.M.; Chandra, D.; Pal, N.K.; Talekar, A.; Lamb, J.; Dolan, M.D.; Paglieri, S.N.; Flanagan, T.B. Phase transformation and crystallization Kinetics of melt-spun Ni₆₀Nb₂₀Zr₂₀ amorphous alloy. *J. Non-Cryst. Solids* **2012**, *358*, 1165–1170.
18. Adam, J.; Rogers, M.D. The crystal structure of ZrO₂ and HfO₂. *Acta Cryst.* **1959**, *12*, 951.
19. Smith, D.K.; Newkirk, H.W. The crystal structure of baddeleyite (monoclinic ZrO₂) and its relation to the polymorphism of ZrO₂. *Acta Cryst.* **1965**, *18*, 983–991.
20. Trufer, G. The crystal structure of tetragonal ZrO₂. *Acta Cryst.* **1962**, *15*, 1187.
21. Yan, Z.J.; Li, J.F.; He, S.R.; Zhou, Y.H. The relation between formation of compounds and glass forming ability for Zr-Al-Ni alloys. *Mater. Lett.* **2003**, *57*, 1840–1843.
22. Kirkpatrick, M.E.; Smith, J.F.; Larsen, W.L. Structure of the intermediate phases Ni₁₀Zr₇ and Ni₁₀Hf₇. *Acta Cryst.* **1962**, *15*, 894–903.
23. Paolone, A.; Cordero, F.; Cantelli, R.; Costa, G.A.; Artini, C.; Vecchione, A.; Gombos, M. Magnetoelastic coupling in RuSr₂GdCu₂O₈. *J. Magn. Magn. Mater.* **2004**, *272–276*, 2106–2107.

24. Paolone, A.; Cantelli, R.; Scrosati, B.; Reale, P.; Ferretti, M.; Masquelier, C. Comparative study of the phase transition of $\text{Li}_{1+x}\text{Mn}_{2-x}\text{O}_4$ by anelastic spectroscopy and differential scanning calorimetry. *Electrochem. Commun.* **2006**, *8*, 113–117.
25. Jayalakshmi, S.; Fleury, E. High temperature mechanical properties of rapidly quenched $\text{Zr}_{50}\text{Ni}_{27}\text{Nb}_{18}\text{Co}_5$ amorphous alloy. *Met. Mater. Int.* **2009**, *15*, 701–711.
26. Jayalakshmi, S.; Park, S.O.; Kim, K.B.; Fleury, E.; Kim, D.H. Studies on hydrogen embrittlement in Zr- and Ni-based amorphous alloys. *Mater. Sci. Eng. A* **2007**, *449–451*, 920–923.
27. Fukuhara, M.; Fujima, N.; Oji, H.; Inoue, A.; Emura, S. Structures of the icosahedral clusters in Ni-Nb-Zr-H glassy alloys determined by first-principles molecular dynamics calculations and XAFS measurements. *J. Alloys Comps.* **2010**, *497*, 182–187.
28. Okamoto, H. H-Zr (Hydrogen-Zirconium). *J. Phase Equilib. Diff.* **2007**, *27*, 548–549.
29. Zuze K.E.; Abriata, J.P. The H-Zr (Hydrogen-Zirconium) system. *Bull. Alloy phase Diagram.* **1990**, *11*, 385–395.
30. Pan, Z.L.; Puls, M.P. Precipitation and dissolution of hydrides in Zr-2.5Nb during quasistatic thermal cycles. *J. Alloys Comps.* **2000**, *310*, 214–218.
31. Pan, Z.L.; Wang, N.; He, Z. Measurements of elastic modulus in Zr alloys For CANDU applications. In Proceedings of 11th International Conference on CANada Deuterium Uranium Fuel, Niagara Falls, ON, Canada, 17–20 October 2010.
32. Palumbo, O.; Paolone, A.; Rispoli, P.; Cantelli, R.; Autrey, T. Decomposition of NH_3BH_3 at sub-ambient pressures: A combined thermogravimetry–differential thermal analysis–mass spectrometry study. *J. Power Sources* **2010**, *195*, 1615–1618.
33. Teocoli, F.; Paolone, A.; Palumbo, O.; Navarra, M.A.; Casciola, M.; Donnadio, A. Effects of water freezing on the mechanical properties of Nafion membranes. *J. Polym. Sci. Part B Polym. Phys.* **2012**, *50*, 1421–1425.
34. Scipioni, R.; Gazzoli, D.; Teocoli, F.; Palumbo, O.; Paolone, A.; Ibris, N.; Brutti, S.; Navarra, M.A. Preparation and characterization of nanocomposite polymer membranes containing superacidic SnO_2 additives. *Membranes* **2014**, *4*, 123–142.
35. Vitucci, F.M.; Manzo, D.; Navarra, M.A.; Palumbo, O.; Trequattrini, F.; Panero, S.; Bruni, P.; Croce, A.; Paolone, A. Low temperature phase transitions of 1-Butyl-1-methylpyrrolidinium bis(trifluoromethanesulfonyl)imide swelling a PVdF electrospun membrane. *J. Phys. Chem. C* **2014**, *118*, 5749–5755.
36. Palumbo, O.; Trequattrini, F.; Vitucci, F.M.; Bianchin, A.; Paolone, A. Study of the hydrogenation/dehydrogenation process in the Mg-Ni-C-Al system. *J. Alloys Compd.* **2015**, doi:10.1016/j.jallcom.2014.12.252.